Optical absorption parameters of amorphous carbon films from Forouhi–Bloomer and Tauc–Lorentz models: a comparative study

2008 J. Phys.: Condens. Matter 20 015216

(http://iopscience.iop.org/0953-8984/20/1/015216)

IOP Publishing Journal of Physics: Condensed Matter

J. Phys.: Condens. Matter **20** (2008) 015216 (8pp) doi:10.1088/0953-8984/20/01/015216

Optical absorption parameters of amorphous carbon films from Forouhi–Bloomer and Tauc–Lorentz models: a comparative study

N Laidani[1,3], R Bartali[1], G Gottardi[1], M Anderle[1] and P Cheyssac[2]

[1] Fondazione Bruno Kessler—Ricerca Scientifica e Tecnologica, Via Sommarive, 18, 38050 Povo (Trento), Italy

[2] Laboratoire de Physique de la Matière Condensée (UMR CNRS 6622), Université de Nice Sophia-Antipolis, Parc Valrose, 06108 Nice cedex 2, France

E-mail: laidani@fbk.eu

Received 18 October 2007, in final form 12 November 2007
Published 7 December 2007
Online at stacks.iop.org/JPhysCM/20/015216

Abstract

Parametrization models of optical constants, namely Tauc–Lorentz (TL), Forouhi–Bloomer (FB) and modified FB models, were applied to the interband absorption of amorphous carbon films. The optical constants were determined by means of transmittance and reflectance measurements in the visible range. The studied films were prepared by rf sputtering and characterized for their chemical properties. The analytical models were also applied to other optical data published in the literature pertaining to films produced by various deposition techniques. The different approaches used to determine important physical parameters of the interband transition yielded different results. A figure-of-merit was introduced to check the applicability of the models and the results showed that FB modified for an energy dependence of the dipole matrix element adequately represents the interband transition in the amorphous carbons. Further, the modified FB model shows a relative superiority over the TL ones for concerning the determination of the band gap energy, as it is the only one to be validated by an independent, though indirect, gap measurement by x-ray photoelectron spectroscopy. Finally, the application of the modified FB model allowed us to establish some important correlations between film structure and optical absorption properties.

(Some figures in this article are in colour only in the electronic version)

1. Introduction

Thanks to their many useful properties such as mechanical resistance, chemical inertness and low friction, amorphous carbon films (hydrogenated or unhydrogenated diamond-like and polymer-like) can cover a broad range of applications. These materials are also attractive candidates as host matrices for the incorporation of nanocrystalline metals. These nanocomposites, with carbon-based matrices instead of transparent media like SiO_2 or Al_2O_3, are of interest for applications in photonic devices [1–3]. Such carbon-based nanocomposites exhibit interesting properties like surface plasmon resonance and field emission properties. They have also been proposed as solar absorber materials [4]. However, in contrast to the other dielectrics, amorphous carbons are a class of materials with a wide range of optical and dielectric properties due to a structure formed by atoms with different degrees of electron hybridization and affected by different kinds of disorder; the properties are tightly correlated with the film synthesis conditions. Consequently, an accurate knowledge of the properties of the carbonaceous matrix is of considerable importance for designing carbon-based nanocomposites with specific performances.

Generally, evaluation of the optical absorption of amorphous insulators and semiconductors requires the parametriza-

[3] Author to whom any correspondence should be addressed.

tion of the photon energy dependence of the optical constants (refractive index, extinction coefficient, dielectric function). Several models have been developed to describe the electronic transition parameters such as the band gap, the peak transition energy and the transition lifetime. These models, namely the Tauc [5], Tauc–Lorentz (TL) [6] and Forouhi–Bloomer (FB) [7] models, are widely applicable. They have been applied to amorphous carbon films too; however, few studies have been made to check their validity in the case of this particular class of materials [8, 9]. It is worthwhile noting that these kinds of studies received new interest in recent works for high-k [10] and amorphous chalcogenide [11] and indium nitride films [12] for example.

In this work, hard amorphous carbon films (a-C) were prepared by rf sputtering and characterized from structural and optical points of view. Application of TL and FB parametrization models was made to the optical constants, with the introduction of a figure-of-merit based on the equality of the peak transition energy and the maximum absorption energy derived from the models. The results show the adequacy of the FB model to describe the interband transition provided that an energy dependence of the dipole matrix element of the transition is introduced. The self-consistency of the model is thus achieved not only for the sputtered films of this study but also for other films from the literature. Furthermore, the application of the modified FB model allowed us to establish some important correlations between film structure and optical absorption properties.

2. Experimental details

2.1. Film deposition

The amorphous carbon films were sputter-deposited from graphite in 5 Pa rf (13.56 MHz) discharges in an Ar–H_2 mixture containing from 0 to 84% H_2 and with a total gas flux of 30 sccm. The samples were mounted on a rotating support, water-cooled to room temperature, and at a distance of 8 cm from the cathode. In order to obtain different C/H compositions and network structures in the films, various plasma energy conditions were applied, either through the variation of the feed gas composition when a plasma was created with a continuous rf wave (CW) [13], or through the modulation of the rf discharge for a given feed gas composition [14]. The rf discharge modulation was achieved by pulsing with 1–100 kHz frequencies. For the CW plasmas, a constant −550 V dc self-bias of the cathode was maintained. The modulated discharges were also produced with −550 V discharge voltage either during the 'time on' of the pulse with a 0 V 'time off' value, or as an average over the 'on' and 'off' times of the pulse.

As the present work focuses only on the applicability of different parametrization models for optical constants of a wide set of carbon films, no weight is directly given to the effects of the process parameters themselves on the film structure. More details of such study can be found in [13–15].

Three kinds of substrate were used: 175 μm thick polyethylene terephthalate (PET) sheets and 1.02 mm thick polycarbonate sheets for optical analysis, both supplied by Goodfellow and n-type Si(100) wafers for chemical analysis. Series of samples were prepared with various film thicknesses, ranging from ∼50 to ∼500 nm.

2.2. Film characterization

X-ray photoelectron spectroscopy (XPS) spectra were recorded with a Scienta ESCA 200 spectrometer and the monochromatized Al Kα (1486.6 eV) radiation. Spectra from survey and detailed scans were recorded, and after a Shirley-type background subtraction raw spectra were fitted using a non-linear fitting program adopting a Gaussian–Lorentzian peak shape. For the valence band spectra, a linear background subtraction was applied. A highly oriented pyrolytic graphite (HOPG) standard sample as well as a standard diamond film [16] were also analysed.

Optical absorption measurements were made with a Jasco V-550 spectrophotometer in the 400–800 nm wavelength range. Reflectance spectra were recorded in the visible range, at normal incidence. An Al mirror was used as a 100% reflectance reference material. Before measuring the sample reflectance, a second Al mirror was measured with respect to the first one in order to assess the experimental measurement error, which was found as 0.5%. Transmittance spectra of samples have also been measured taking the bare substrate as reference.

Fourier-transform infra-red spectroscopy (FT-IR) was used to quantify the chemically bound hydrogen content of the films. It was carried out with a Bio-Rad FTS 185 spectrometer equipped with a DTGS detector and a KBr beam splitter, in the absorbance mode and within the 400–4000 cm^{-1} wavenumber range. In particular the 2600–3200 cm^{-1} interval was considered. This corresponds to the stretching vibration modes of various C–H bonds and allows us to determine the composition of the hydrogenated phase of the film structure.

3. Results

3.1. Background

Optical absorption measurements are widely used to characterize the electronic properties of materials, through the determination of parameters describing the electronic transitions such as: band gap, valence band tails and lifetime of the excited state, which can be related to disorder in the material network, i.e. bond strength and defects. However, the optical absorption depends not only on a convolution of the density of states of the conduction and valence bands (CB and VB), but also on the matrix elements of electronic transitions. From optical properties alone it is not possible to uniquely determine electronic properties without simplifying assumptions about these matrix elements and the density of states.

From the quantum mechanics of optical absorption, within the one-electron approximation, it is shown that the imaginary part $\varepsilon_2(E)$ of the relative dielectric function is

$$\varepsilon_2(E) = \left(\frac{2\pi e\hbar}{m}\right)^2 \left(\frac{2}{VE^2}\right) \sum |P_{v,c}|^2 \delta(E_c - E_v - E) \quad (1)$$

where E is the energy of the incident light wave, V is the illuminated volume, e and m are the electron charge and mass, respectively, E_v is the energy of the initial (valence) state and E_c is that of the final (conduction) state. $|P_{v,c}|^2$ is the square of the momentum matrix element associated with the transition. (Note that we use in this work interchangeably the terms 'initial' and 'valence' as well as 'final 'and 'conduction' for the states involved in the transition.)

Equation (1) can be equivalently rewritten in terms of the squared dipole matrix element, $|R_{v,c}|^2$, as

$$\varepsilon_2(E) = (2\pi e)^2 \left(\frac{2}{V}\right) \sum |R_{v,c}|^2 \delta(E_c - E_v - E). \quad (2)$$

Several models are commonly used to determine the optical properties of amorphous semiconductors and dielectrics in the energy range of interband transitions. The most widespread is the Tauc model [5] which allows us to derive the band gap energy E_g from $E\sqrt{\varepsilon_2}$ as a function of the incident energy E. E_g is then obtained by extrapolating $E\sqrt{\varepsilon_2}$ to zero, according to $E\sqrt{\varepsilon_2} = B_T(E - E_g)$. Tauc's approximation considers a parabolic behaviour of the bands near the edge; B_T is a constant and the square of the average matrix element of the dipolar momentum

$$P^2(E) = |P_{v,c}|^2 = |\langle c|p|v\rangle|^2$$

is assumed to be independent of the photon energy E.

In the Tauc–Lorentz model, introduced by Jellison and Modine [6], $\varepsilon_2(E)$ is given as the product of the Tauc function: $G(E)\alpha\frac{E-E_g}{E^2}$ by the Lorentz oscillator function $L(E)$:

$$L(E) = AE_0\Gamma E/[(E^2 - E_0^2) + \Gamma^2 E^2].$$

Hence

$$\varepsilon_2(E) = \frac{1}{E}\frac{AE_0\Gamma(E - E_g)^2}{\left[(E^2 - E_0^2)^2 + \Gamma^2 E^2\right]} \qquad \text{for } E > E_g \quad (3a)$$

and

$$\varepsilon_2(E) = 0 \qquad \text{for } E \leqslant E_g. \quad (3b)$$

A is the amplitude factor, proportional to the density of the material and to the momentum matrix element. E_0 is the peak transition energy that corresponds to the so-called Penn gap. Γ is the broadening parameter, inversely related to short-range order [17] and crystallite size [18].

Similarly to the TL model, in Forouhi and Bloomer's formalism important parameters such as the transition lifetime τ, the energy gap between the top of the valence band and the bottom of the conduction band and the peak transition energy can be derived [7, 19]. This is achieved by fitting the extinction coefficient, i.e. the imaginary part $\kappa(E)$ of the refractive index, with

$$\kappa(E) = A(E - E_g)^2/(E^2 - BE + C), \quad (4)$$

where A, is related to the transition dipole matrix element as

$$A \propto \frac{1}{\tau}|\langle c|x|v\rangle|^2, \quad (5)$$

$$B = 2(E_c - E_v) \quad (6)$$

and

$$C = (E_c - E_v)^2 + \hbar^2/4\tau^2. \quad (7)$$

Here $(E_c - E_v) = B/2$ corresponds to the maximum absorption (or Penn gap, as in the case of E_0 in the TL model).

Although both TL and FB models are based on the assumption of parabolic VB and CB band edges, they differ from each other in the assumption of the matrix element energy dependency: in the FB model the squared dipole matrix element is considered as constant with energy variation

$$R^2(E) = |\langle c|x|v\rangle|^2 \quad (8)$$

where 'x' is for position.

The same limitation is recalled for both FB and TL models: a non-zero absorption in amorphous semiconductors at energies below the energy gap. Actually, when $E < E_g$, there exists a tail called the Urbach tail due to disorder of the amorphous network [20, 21]; this sub-gap energy range will not be considered in the present study.

Knowing the relation between $P^2(E)$ and $R^2(E)$, given by

$$P^2(E) = \frac{m^2}{\hbar^4}E^2R^2(E), \quad (9)$$

it becomes important to know which approximation of an energy-independent matrix element holds for a given material. In this work, we have studied the applicability of existing models for the optical transitions in amorphous carbon films, with the introduction of a figure-of-merit that allows the adequacy of the model to be checked, with a further validation of the electron properties through an independent characterization by a non-optical method.

3.2. Calculation of optical constants from transmittance and reflectance spectra

Most of the studied films were sufficiently absorbing to give transmittance spectra without interference patterns characteristic of multiple reflections at the various interfaces in the film + substrate system. For such films, the imaginary part κ of the complex index $\nu + i\kappa$ was calculated using $\kappa = \alpha\lambda/4\pi$, the absorption coefficient α being given by

$$\alpha = \frac{1}{t}\,\mathrm{Ln}\left(\frac{1 - R}{T}\right), \quad (10)$$

where λ is the wavelength, t the film thickness and T and R the transmittance and reflectance, respectively. At normal incidence in air, the reflectance R of an absorbing medium of refraction index $\nu + i\kappa$ is given by $R = \frac{(\nu-1)^2+\kappa^2}{(\nu+1)^2+\kappa^2}$; then the real part ν of the index was extracted from its values. In figure 1(a) two examples of absorption coefficients of films deposited in two kinds of plasmas: one of pure Ar and the other of an Ar (84%)–H_2 (16%) mixture, are given as a function of wavelength.

The reflectance spectra of some samples showed interference patterns in a narrow interval corresponding to the

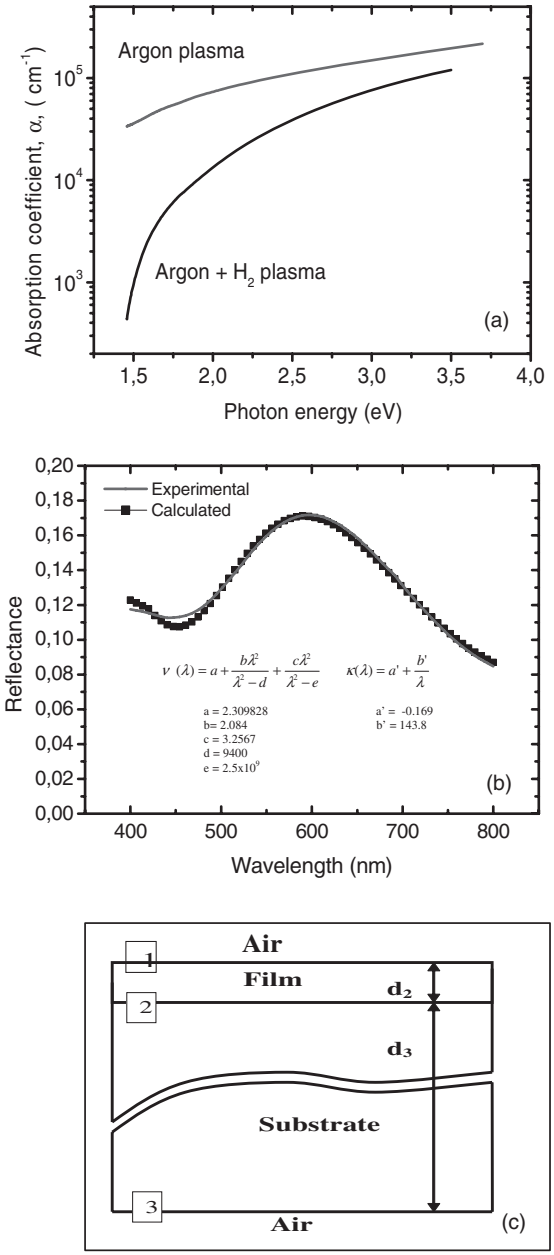

Figure 1. (a) Examples of absorption coefficients of films deposited in Ar and Ar–H_2 (84–16)% plasmas as a function of wavelength. (b) Experimental and calculated reflectance spectra of a-C film on polycarbonate in the case of multiple reflections. (c) Schematic multilayered structure of the a-C/polycarbonate system.

highest wavelengths. In the remaining range of wavelengths, ν and κ were determined using the procedure described above.

Few films, though giving transmittance spectra without evident interference, still presented such patterns in their reflectance spectra over the entire wavelength range. A typical spectrum is presented in figure 1(b). In such a case we proceeded as follows: two series of reflectance spectra were measured, one with the rear face of the substrate kept bare as for all samples described above, and the other with the rear face of the substrate coated by a black absorbing layer of graphite. The purpose of the latter procedure was to minimize the reflection due to the rear face of the rather thick polycarbonate sheet. For such a configuration, the optical constants were then calculated more easily by fitting the reflectance spectrum. Here we give the procedure adopted for a 211 nm thick film deposited on a polycarbonate substrate, a structure sketched in figure 1(c).

The amplitude of the electric field reflected by the sample is described according to the classical principles of propagation of electromagnetic waves, discussed by Born and Wolf [22]: namely we consider a plane and parallel layer of carbon deposited on a semi-infinite substrate of polycarbonate and so we define three interfaces: (1) air/film, (2) film/substrate and (3) substrate/air (figure 1(c)). Since the rear face of polycarbonate is coated and absorbing, no wave is back-reflected; the combination of interfaces becomes rather straightforward, although complex values of indices have to be handled with care.

Let n_i be the index of the ith layer. The reflectance coefficients ρ_{ij} of the various interfaces are $\rho_{ij} = \frac{n_i - n_j}{n_i + n_j}$ with ρ_{12} for the vacuum–carbon layer, and ρ_{23} for carbon–polycarbonate. Then, the theoretical expression of Fresnel reflectance is $R_{\text{Fresnel}} = \rho\rho^*$ with

$$\rho = \frac{\rho_{12} + \rho_{23} e^{2ik_2 d_2}}{1 + \rho_{12}\rho_{23} e^{2ik_2 d_2}}, \tag{11}$$

where k_2 is the wavevector and d_2 the thickness of the carbon layer [23]. Inputs of the calculations are indices for polycarbonate $n_p = \nu_p + i\kappa_p$, the optical index $n = \nu + i\kappa$ of carbon and its measured thickness $d_2 = 211$ nm.

The indices for polycarbonate were derived from a fit of its reflectance curve. Initial guess values for ν and κ of carbon were necessary for the calculations. According to [24], the Sellmeier dependence of diamond was chosen for ν with λ. The wavelength dependence of κ was derived using equation (10) from T and R spectra measured on samples whose substrate was left with a bare rear face. We considered this dispersion as the most realistic one for input values of κ in the calculations. As a result, the fit of R is quite good over most of the energy range, as can be seen in figure 1(b). The wavelength dispersion parameters of $\nu(\lambda)$ and $\kappa(\lambda)$, as obtained from the fit of experimental $R(\lambda)$, are given in the inset of figure 1(b).

In the visible range, the optical properties of all carbon films studied here are then described by the real and imaginary parts of either their index $n = \nu + i\kappa$ or their dielectric function $\varepsilon = \varepsilon_1 + i\varepsilon_2$.

3.3. FB model: self-consistency checking and consequent model modification

The values of optical constants that have been obtained were used to study the absorption properties, i.e. the parameters of electronic transitions of the amorphous carbon films.

$\kappa(E)$ of all samples has been fitted to FB model which allowed us to quantify the transition parameters, in particular the values of the optical gap (E_g) and the peak transition ($B/2$), which will be discussed.

From the parameters of the FB fit, we also derived the energy $E_{\max}$, corresponding to the maximum of absorption (maximum of κ). $E_{\max}$ and $B/2$ should be very close as

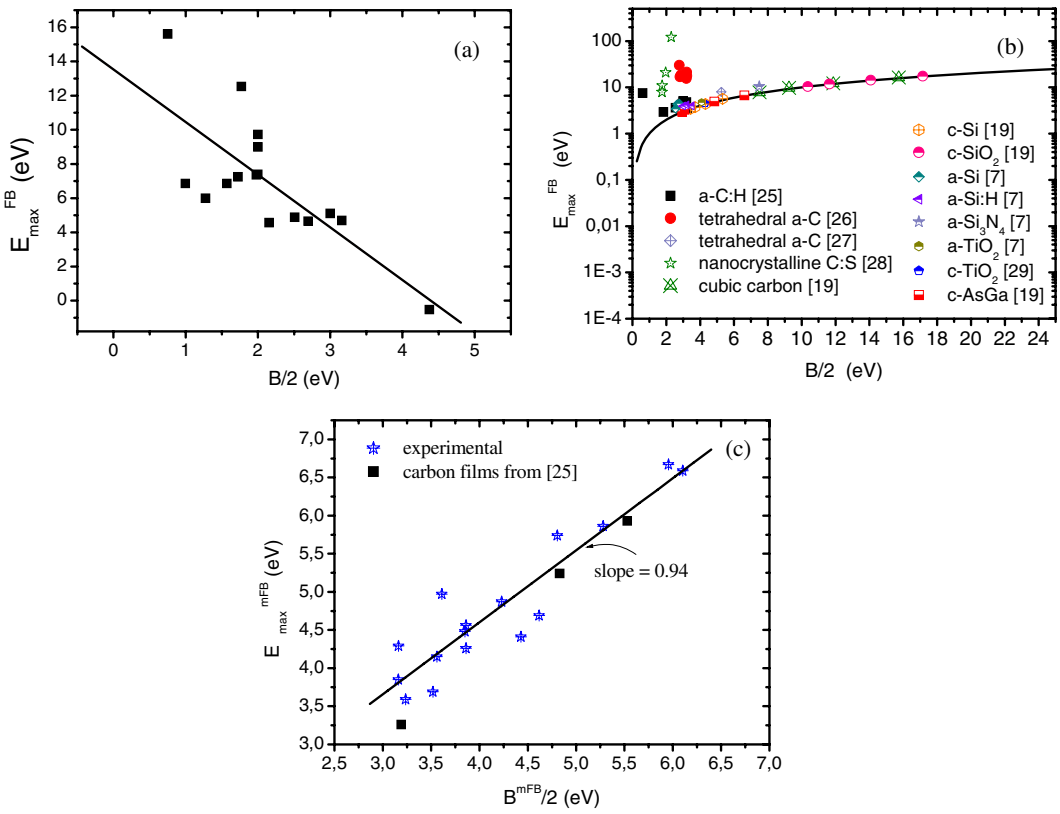

Figure 2. (a) E_{max} versus the energy difference $B/2$ between the final and initial states of a transition; both parameters were determined from the unmodified FB model applied to our carbon films. (b) Semi-log graph of E_{max} versus $B/2$, from the FB model, both parameters were determined from tabulated data. The one-to-one relationship is represented by a solid line. (c) E_{max} versus $B/2$; both parameters were determined from the modified FB (mFB) model applied to our carbon films (star symbols) and to some literature data [33] (square symbols). The latter are represented with the same symbol in plot (b).

they have the same physical significance. So, to check the applicability of the model, we took first the equality of $B/2$ and E_{max} values as a figure-of-merit. The two parameters are plotted in figure 2(a), which clearly shows the lack of correspondence between them, evidenced by the linear fit of the data which gives a negative slope. Furthermore, we found that this inconsistency was not only restricted to carbon films, but these are among the amorphous materials for which FB parametrization is the least applicable. In order to illustrate these remarks, we selected a wide range of amorphous materials and, also for completeness, crystalline materials for which FB fitting parameters of $\kappa(E)$ were available in a tabulated form in literature. The amorphous solids having such available data are a-C:H [25], tetrahedral a-C [26, 27], nanocrystalline-C:S [28], a-Si, a-Si:H, a-Si_3N_4 and a-TiO_2 [7]. The tested crystalline materials were c-GaAs, c-Si, c-SiO_2, diamond [19] and c-TiO_2 [29]. In these cases, all possible transitions were considered.

A semi-log graph of E_{max} versus $B/2$ is displayed in figure 2(b). We can see that the crystalline solids rigorously follow a one-to-one relationship between the two energies, represented by the solid line in the plot, contrary to the amorphous ones which exhibit strong deviations, the most drastic ones being for the amorphous carbon films, as introduced before.

The approximation of an energy-independent dipole matrix element does not make sense when applied to amorphous carbons (figures 2(a) and (b)) or to nanocrystalline carbon (figure 2(b)).

In order to make the FB model tractable with our studied a-C films, we tried another approach that introduces an energy dependence in the squared matrix element $R^2(E)$ of the transition dipole which enters the physical model of FB. The assumption of parabolic band edges has been kept but the sub-gap energy range has been ignored. Our choice of the energy dependence of $R^2(E)$ is based on earlier indications of a E^{-2} energy scaling of matrix elements in disordered materials [20, 30]. We then introduced, as follows, this energy dependence $R^2(E) \propto E^{-2}$ in the FB parametrization:

$$\kappa(E) = \frac{1}{E^2}\frac{A^*(E-E_g)^2}{E^2 - BE + C}. \qquad (12)$$

Using this formulation, the best fit of experimental $\kappa(E)$ with this formulation gave the $B/2$ and E_{max} values which are plotted in figure 2(c) and linearly fitted with a slope of 0.94. The equality of $B/2$ and E_{max} chosen as a figure-of-merit is now fairly achieved.

The modified FB formulation (hereafter mFB) for $\kappa(E)$ versus photon energy has been applied to a series of amorphous hydrogenated carbon films whose optical constants ν and κ are compiled in [25]. From tabulated values for the three films we plotted $\kappa(E)$ and checked, through the $B/2 = E_{max}$ figure-of-merit, the validity of the original model and our modified

FB one (square symbols in figures 2(b) and (c) respectively). As in the case of our films, it is demonstrated that the mFB model is able to describe the absorption properties of such materials.

3.4. Validation of mFB model for amorphous carbons

In order to further validate the applicability of the mFB model to amorphous carbon, we compared two parameters: the value of the optical gap E_g resulting from the $\kappa(E)$ fit and the valence band maximum (VBM) energy measured by XPS. The latter parameter was chosen as an indirect measure of the band gap since we found a strong correlation between these two energies for selected standard carbon-based materials: diamond (i.e. a 100% sp^3 hybridized carbon), graphite (a 100% sp^2 hybridized carbon), polyethylene (a 100% sp^3 hybridized hydrogenated carbon with 66.6 at.% H) and *para*-quaterphenyl which is a polyphenylene oligomer (a 100% sp^2 hybridized hydrogenated carbon, with 42.8 at.% H). A third polymer, poly(*cis*-isoprene), which is a mixed sp^3–sp^2 hydrogenated carbon (60%–40% respectively) and contains 61.5 at.% H, was also considered. In the present study, XPS spectra from diamond and graphite were acquired from standard materials, whereas those belonging to the three polymers were taken from the literature [31]. The valence band (VB) top energy is defined as the energy of the zero-intensity point of the spectrum at the low binding energy side. The latter is obtained by a linear extrapolation of the region of the spectrum of lowest binding energy. In XPS, all spectra, and in particular for this study the VB and C 1s core level ones, were measured with respect to the Fermi level. In order to eliminate any possible effect of a change of Fermi level within the gap, due to different structures and/or different levels of hydrogenation of the films, we used the binding energies of the VB maximum (E_{VBM}) and C 1s core level ($E_{\mathrm{C\ 1s}}$) and took into consideration their difference, $\Delta E = E_{\mathrm{C\ 1s}} - E_{\mathrm{VBM}}$. Typical spectra are displayed in figures 3(a) and (b). $E_{\mathrm{C\ 1s}}$ is taken as the binding energy of the main peak obtained after deconvolution of the C 1s spectrum into individual peaks for the carbon and diamond films and for graphite. For the spectra taken from the literature, $E_{\mathrm{C\ 1s}}$ was simply the energy of the C 1s peak maximum.

The energy difference ΔE should reflect more precisely the red shift of the VB maximum in the case of a gap opening. This was found to be valid for both groups of standard materials, hydrogenated and unhydrogenated carbons. The lower ΔE is, the higher E_g, as is seen in figure 3(c). Optical gaps of reference carbons were taken from the literature [32–35].

In figure 3(d), we report experimental data from optical and XPS measurements on a set of carbon films deposited with various frequency conditions of plasma pulsing in 84 at.% Ar–16 at.% H_2 [14]. One sees that the values of E_g^{mFB} deduced from the mFB model fit this correlation well. The same cannot be said for the original FB model: no such correlation between E_g^{FB} and ΔE is seen in the plot in figure 3(e).

3.5. Comparison between the results of mFB and TL fits

For all studied films, $\varepsilon_2(E)$ has also been fitted to the TL model in order to extract E_g^{TL} and E_0^{TL}, the energies of the optical gap

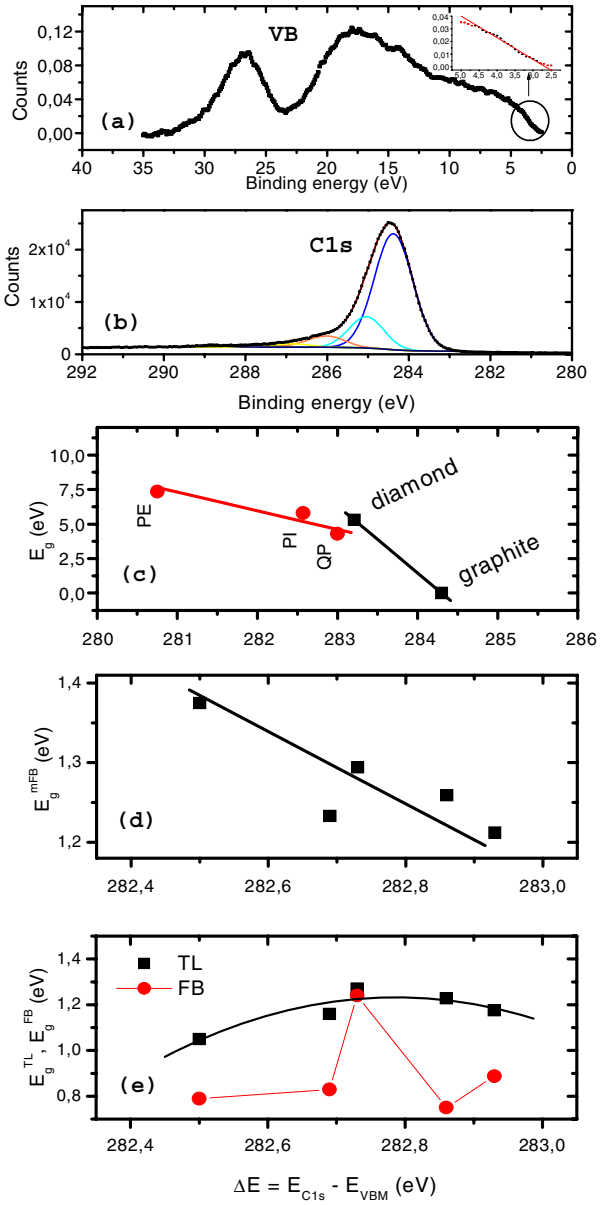

Figure 3. (a) Typical XPS VB spectrum of a-C film. (b) Typical XPS C 1s spectrum of a-C film. (c) Optical gap versus $\Delta E = E_{\mathrm{C\ 1s}} - E_{\mathrm{VBM}}$ for diamond, graphite, polyethylene, *para*-quaterphenyl and polyisoprene (named PE, QP and PI, respectively, in the graph). (d) Optical gap of carbon films derived from the mFB model versus $\Delta E = E_{\mathrm{C\ 1s}} - E_{\mathrm{VBM}}$. (e) Optical gap of carbon films derived from the original FB and from TL models versus $\Delta E = E_{\mathrm{C\ 1s}} - E_{\mathrm{VBM}}$.

and maximum absorption, as well as the transition lifetime and to compare them with their corresponding values in the mFB formulation. Figure 4(a) shows the mutual correspondence between E_0^{TL} and $E_{\mathrm{max}}^{\mathrm{mFB}}$. No fair matching of a one-to-one relationship (represented by a straight line in the figure) is observed between these two parameters. In most cases the values deduced from TL model are larger than those from the mFB one; this is despite the E^{-2} scaling of $R^2(E)$ in the mFB model, which turns out as in the TL model: a squared constant momentum matrix element (see equation (9)). Furthermore, the TL model is much less well validated than the mFB one

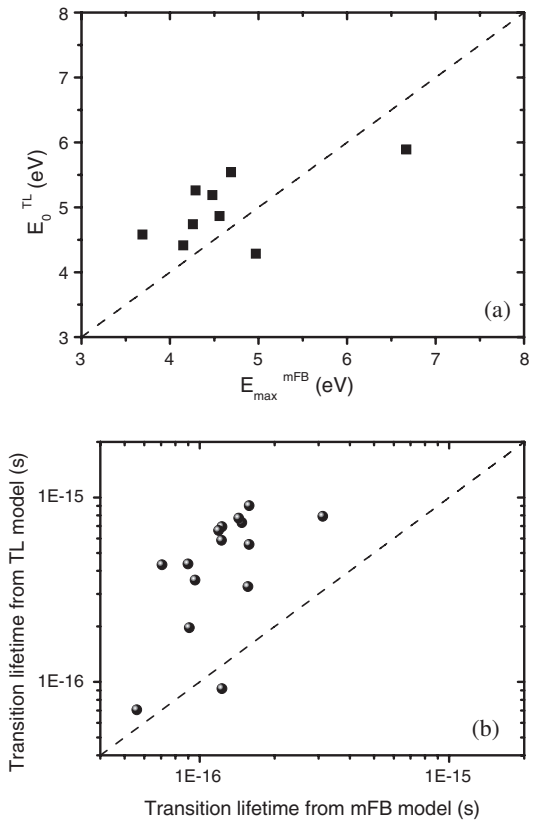

Figure 4. (a) Transition energy, E_0^{TL}, from the TL model versus E_{max}^{mFB} from the mFB model for amorphous carbon films. (b) Transition lifetimes from the TL versus the mFB model.

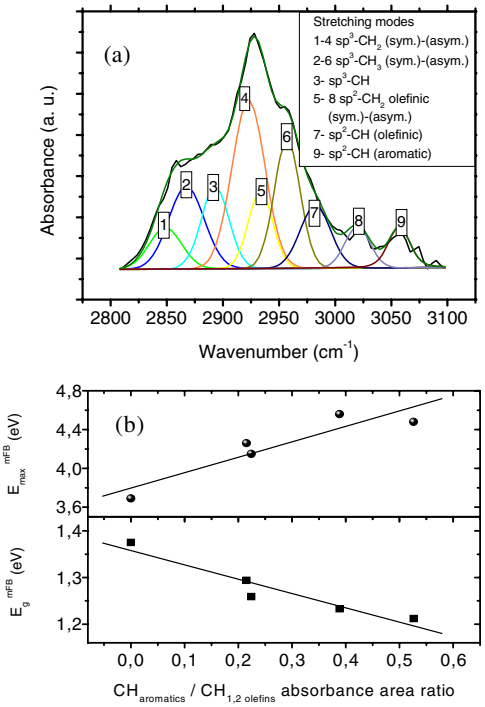

Figure 5. (a) Typical FT-IR spectrum in the 2800–3100 cm^{-1} wavenumber range ('sym.' and 'asym.' stand respectively for symmetric and asymmetric stretching modes). (b) E_g^{mFB} and E_{max}^{mFB} versus the ratio of FT-IR absorption area between aromatic C–H and olefinic C–$H_{1,2}$ bonds.

by the results of XPS measurements. In figure 3(e), the plot of $\Delta E = E_{C\ 1s} - E_{VBM}$ versus E_g^{TL}, as defined in the above section, did not give a similar trend to what has already been described above. At this stage, this shows the relative superiority of mFB model for giving the energy of the optical gap of these amorphous carbons.

The transition lifetime from mFB was derived according to equation (7) from the C value given by the $\kappa(E)$ fit, and that from the TL model was calculated as h/Γ, Γ coming from the $\varepsilon_2(E)$ fit according to equation (3*a*). Here, in most cases transition lifetimes from the TL model came to be higher than those from the mFB one, by up to a factor 10, as shown in figure 4(b).

3.6. Correlations between chemical structure and optical transition parameters of films

The optical properties of amorphous C films are known to be dominated by π–π^* and σ–σ^* electronic transitions, along with π–σ^* and σ–π^* transitions [35, 36]. The π–π^* contribution originates exclusively from sp^2 carbon.

In graphite the π–π^* transition is located at ∼4 eV, whereas the σ–σ^* transitions occur at ∼14 eV, at a higher energy than in diamond (∼11 eV). All these values of energy correspond to the maximum of absorption for a specific interband transition and are not the value of the optical gap which is null for graphite. Moreover, they can be consistently lower in the amorphous materials than in their bulk crystalline counterparts (graphite and diamond in the case of unhydrogenated carbon) [36, 37]. Similarly, the optical gap is used to characterize different kinds of disorder in the structure of amorphous carbon films. It has been shown that the optical gap is controlled by the number of sp^2 sites in the structure but the manner in which this control occurs is still an open subject. A same sp^2 C fraction can result in different optical properties, depending on the local sp^2 configuration. In fact, the existing propositions about the effect of sp^2 C on the gap value are oriented to explain the origin of a 'gap opening'; that is the optical properties of the films are evaluated referring to a perfectly ordered sp^2 structure, which would behave like a zero-gap material such as graphite. The 'gap opening' could therefore be due to the presence of sp^2 C clusters of nanometric size, viewed as graphitic units, and thus due to a size effect which would manifest in a blue shift of the optical gap. Alternatively, as described by the revised structural model of Robertson, the clusters would consist of a ring and chain bonding configuration rather than condensed aromatic nuclei in 'graphitic units' [35].

Let us recall that the sp^2 C phase is the one susceptible to giving rise to absorption in the visible energy range. The mFB model, yielding a more precise knowledge of peak transition and optical gap energies, allows us to establish correlations between these important parameters and the structure of the materials. In the present case we investigated the effect of the chemical structure, as determined by FT-IR analysis of the same series of films used to validate the model by XPS. In particular, we focused on the C–H_x stretching vibrational band. A typical spectrum is presented in figure 5(a), with

its deconvolution into Gaussian individual peaks identified according to published data [38], as shown in the inset of the figure. This way, the hydrogenated sp^2 C phase was found to be due to both aromatic and olefinic carbon, i.e. carbon atoms organized in rings and in chains, respectively, in proportions varying with the parameters of the film deposition process.

A strong effect of the composition of the hydrogenated sp^2 carbon phase on the film optical gap and peak transition energies was found. Plotting E_g^{mFB} and E_{max}^{mFB} versus the ratio of sp^2 ring-to-sp^2 chain band areas, i.e. the area of aromatic sp^2 CH band, labelled '9' in figure 5(a), ratioed to the area sum of olefinic sp^2 CH_2 + sp^2 CH bands (peaks '8' and '7'), puts clearly in evidence the role of the chain bonds in the gap opening and the red shift of the absorption peak. This is illustrated in figure 5(b): the higher the proportion of chain bonds (the lower the ring one) the larger the gap, E_g^{mFB}, and the lower the energy, E_{max}^{mFB}, of peak transition, meaning thereby a narrowing of the valence band.

4. Conclusion

In this work, the optical properties of amorphous carbon films have been studied. The goal was to define the parameters of important interband absorption such as band gap and peak transition energies and transition lifetime. The Tauc–Lorentz and Forouhi–Bloomer commonly used analytical models were applied to the film optical constants. The inconsistency of the FB model when applied to amorphous carbons was evidenced. A modification of the FB model made by introducing an energy dependence of the dipole matrix element (as $\propto E^{-2}$) turns out to be more adequate to describe the interband transition in a-C and a-C:H films, whereas the original FB model was found to be well-suited for many other amorphous non-carbonaceous semiconductors and insulators. Furthermore, the modified FB model shows a relative superiority over the TL one concerning the determination of the band gap energy, as it is the only one to be validated by measurements by XPS of the valence band edge energy itself related to the bandgap. Finally, the application of the modified FB model allowed us to establish some important correlations between the film structure and its optical absorption properties.

Acknowledgments

This work was supported by Autonomous Province of Trento (Fondo Progetti Ricerca) under the project MicroCombi. Many thanks to V Micheli for technical assistance.

References

[1] Hussain S and Pal A K 2007 *Appl. Surf. Sci.* **253** 3469
[2] Hussain S, Roy R K and Pal A K 2005 *J. Phys. D: Appl. Phys.* **38** 900
[3] Kundoo S, Saha P and Chattopadhyay K K 2004 *J. Vac. Sci. Technol.* B **22** 2709
[4] Schuler A, Geng J, Oelhafen P, Brunold S, Gantenhein P and Frei U 2000 *Sol. Energy Mater. Sol. Cells* **60** 295
[5] Tauc J, Grigorovici R and Vancu A 1966 *Phys. Status Solidi* **15** 627
[6] Jellison G E Jr and Modine F A 1996 *Appl. Phys. Lett.* **69** 371
[7] Forouhi A R and Bloomer I 1986 *Phys. Rev.* B **34** 7018
[8] Mc Gahan W A, Makovicka T, Hale J and Woollam J A 1994 *Thin Solid Films* **253** 57
[9] Yamaguchi T, Kaneko Y, Jayatissa A H and Aoyama M 1996 *Thin Solid Films* **279** 174
[10] Price J, Hung P Y, Rhoad T, Foran B and Diebold A C 2004 *Appl. Phys. Lett.* **85** 1701
[11] Ohlidal I, Franta D, Siler M, Vizd'a F, Frumar M, Jedelsky J and Omasta J 2006 *J. Non-Cryst. Solids* **352** 5633
[12] Khoshman J M and Kordesch M E 2006 *J. Non-Cryst. Solids* **352** 5572
[13] Laidani N, Bartali R, Tosi P and Anderle M 2004 *J. Phys. D: Appl. Phys.* **37** 2593
[14] Laidani N, Bartali R, Anderle M, Chiggiato P and Chuste G 2005 *Diamond Relat. Mater.* **14** 1023
[15] Calliari L, Filippi M, Laidani N and Anderle M 2006 *J. Electron Spectrosc.* **150** 40
[16] Filippi M, Calliari L, Pucella G and Verona-Rinati G 2004 *Surf. Sci.* **573** 225
[17] Pereira L, Āguas H, Fortunato E and Martins R 2006 *Appl. Surf. Sci.* **253** 339 and references therein
[18] Feng G F and Zallen R 1989 *Phys. Rev.* B **40** 1064
[19] Forouhi A R and Bloomer I 1988 *Phys. Rev.* B **38** 1865
[20] Connel G A N 1979 *Optical Properties in Amorphous Semiconductors* (*Springer Topics in Applied Physics, Amorphous Semiconductors* vol 36) ed M H Brosky (Berlin: Springer) pp 73–111
[21] Miranda C R, Antonelli A, da Silva A J R and Fazzio A 2004 *J. Non-Cryst. Solids* **338–340** 400
[22] Born M and Wolf E 1999 *Principles of Optics* 7th edn (Cambridge, MA: Cambridge University Press)
[23] Cheyssac P 2006 *Opt. Commun.* **268** 273
[24] Ghosh G 1998 *Handbook of Thermo-optics Coefficients of Optical Materials with Applications* (New York: Academic) pp 5–110
[25] Alterovitz S A, Savvides N, Smith F W and Woollam J A 1998 *Handbook of Optical Constants of Solids* ed A D Palik (New York: Academic) pp 837–852
[26] Xu S, Cheah L K and Tay B K 1998 *Thin Solid Films* **312** 160
[27] Canillas A, Polo M C, Abdujar J L, Sancho J, Boch S, Robertson J and Milne W I 2001 *Diamond Relat. Mater.* **10** 1132
[28] Gupta S, Weiner B R and Morell G 1998 *Thin Solid Films* **455/456** 422
[29] Chryscopoulos P, Davazoglu D, Trapalis C and Kordas G 1998 *Thin Solid Films* **323** 188
[30] Fanchini G and Tagliaferro A 2001 *Diamond Relat. Mater.* **10** 191 and references therein
[31] Moulder J F, Stickle W F, Sobol P E and Bomber K D 1995 *Handbook of X-ray Photoelectron Spectroscopy* ed J Chastaing and R C King Jr (Eden Prairie, MN: Physical Electronics)
[32] Tanaka T 1973 *J. Appl. Phys.* **44** 2430
[33] Bredas J L, Themans B, Fripiat J G, André J M and Chance R R 1984 *Phys. Rev.* B **29** 6761
[34] Najidha S, Saxena N S, Sreeja R, Unnithan C H and Predeep P 2005 *Mater. Lett.* **59** 3431
[35] Robertson J 2002 *Mater. Sci. Eng.* R **37** 129
[36] Logothetidis S 2003 *Diamond Relat. Mater.* **12** 141
[37] Giri P K, Tripurasundari S, Raghavan G, Panigrahi B K, Magudapathy P, Nair K G M and Tyagi A K 2001 *J. Appl. Phys.* **90** 659
[38] Colthup N B, Daly L H and Wiberley S E 1969 *Introduction to Infrared and Raman Spectroscopies* (New York: Academic)